Inorg. Chem. **2008**, *47*, 4785−4795

Reactivity of a Phosphinito-Bridged $Pt^{I}-Pt^{I}$ Complex with Nucleophiles: Substitution versus Addition

Vito Gallo,[†] Mario Latronico,[†] Piero Mastrorilli,*[,†] Cosimo F. Nobile,[†] Flavia Polini,[†] Nazzareno Re,[‡] and Ulli Englert[§]

Dipartimento di Ingegneria delle Acque e di Chimica del Politecnico di Bari, via Orabona 4, I-70125 Bari, Italy, Dipartimento di Scienze del Farmaco, Università "G. d'Annunzio", Via dei Vestini 31, I-06100 Chieti, Italy, and Institut für Anorganische Chemie der RWTH, Landoltweg 1, D-52074 Aachen, Germany

Received January 15, 2008

As a result of the strong electrophilic character of the Pt bound to O, the phosphinito-bridged Pt^{I} complex [$(PHCy_2)Pt(\mu$-$PCy_2)\{\kappa^2P,O$-μ-$P(O)Cy_2\}Pt(PHCy_2)$]($Pt-Pt$) (**1**) undergoes attack at the O-bound Pt atom by molecules such as di- and tricyclohexylphosphane, dicyclohexylphosphane oxide, and dicyclohexylphosphane sulfide. Thus, reaction of **1** with $PHCy_2$ gives the symmetric Pt^{I} dimer [$(PHCy_2)Pt(\mu$-$PCy_2)]_2$($Pt-Pt$) (**2**), while the hydrido-bridged complex *syn*-[$(PHCy_2)\{\kappa P$-$P(O)Cy_2\}Pt(\mu$-$PCy_2)(\mu$-$H)Pt(PHCy_2)\{\kappa P$-$P(O)Cy_2\}$]($Pt-Pt$) (**4**) is obtained from reaction of **1** with $P(O)HCy_2$; the thiophosphinito complex [$(PHCy_2)Pt(\mu$-$PCy_2)\{\kappa^2P,S$-μ-$P(S)Cy_2\}Pt(PHCy_2)$]($Pt-Pt$) (**8**) forms selectively in reaction of **1** with $P(S)HCy_2$. For comparison, the reaction with PCy_3 results only in ligand substitution, affording [$(PCy_3)Pt(\mu$-$PCy_2)\{\kappa^2P,O$-μ-$P(O)Cy_2\}Pt(PHCy_2)$]($Pt-Pt$) (**5**). DFT studies confirmed the remarkable electrophilicity of the oxygen-bound Pt and shed light on the nature of the metal−metal bond in Pt dimers.

Introduction

We have recently described the synthesis of [$(PHCy_2)Pt^1(\mu$-$PCy_2)\{\kappa^2P,O$-μ-$P(O)Cy_2\}Pt^2(PHCy_2)$]($Pt-Pt$) (**1**), a rare example of an asymmetric monophosphido-bridged complex with Pt atoms in the formal oxidation state +1.[1] Although no solid-state structure was reported, multinuclear NMR features allowed us to infer a bridging coordination mode of the $P(O)Cy_2$ ligand. The valence electron count of 30 for **1** indicates the presence of a Pt−Pt bond, in agreement with the diamagnetic character of the $Pt^{I}-Pt^{I}$ complex. The $^{195}Pt\{^1H\}$ NMR spectrum did not show any coupling between the Pt atoms, which was an odd circumstance in view of the results obtained for related unsymmetrical $Pt^{I}-Pt^{I}$ dimers, where coupling constants of 337,[1] 512,[2] or 1552 Hz[3] were observed. The fact that satellites stemming from the isotopomer having two ^{195}Pt atoms were absent from the $^{195}Pt\{^1H\}$ NMR spectrum suggested that the molecule might rather be considered as a $Pt^{II}-Pt^{0}$ system, with a Pt−Pt bond endowed with a low s character. Moreover, the ^{195}Pt NMR chemical shifts [$\delta_{Pt(1)} = -4798$, $\delta_{Pt(2)} = -5205$] indicated significantly different electron densities for the two Pt atoms, suggesting an electrophilic character for Pt^1 (the Pt bonded to O).

Intrigued by this view, which paves the way to a wide and unexplored reactivity, we have studied the electronic structure of **1** by X-ray diffraction (XRD) and density functional theory (DFT) and investigated the reactivity of **1** with suitable nucleophiles, such as $PHCy_2$, PCy_3, $P(O)HCy_2$, and $P(S)HCy_2$.

Results and Discussion

XRD Structure of 1. The structure of **1** is reported in Figure 1 and confirms our previous assignments made on the basis of IR, NMR, high-resolution (HR) electrospray ionization mass spectrometry (ESI−MS), and elemental analyses. In particular, the complex features a $P(O)Cy_2$ ligand bridging two Pt atoms that are joined by a Pt−Pt single bond [2.5731(16) Å] and further bridged by a dicyclohexylphosphide ligand. The coordination sphere of each platinum is completed by a $PHCy_2$ ligand trans to the Pt−Pt bond. The

* To whom correspondence should be addressed. E-mail: p.mastrorilli@poliba.it.
† Politecnico di Bari.
‡ Università "G. d'Annunzio".
§ Institut für Anorganische Chemie der RWTH.

(1) Gallo, V.; Latronico, M.; Mastrorilli, P.; Nobile, C. F.; Suranna, G. P.; Ciccarella, G.; Englert, U. *Eur. J. Inorg. Chem.* **2005**, 4607–4616.
(2) Cittadini, V.; Leoni, P.; Marchetti, L.; Pasquali, M.; Albinati, A. *Inorg. Chim. Acta* **2002**, *330*, 25–32.
(3) Bender, R.; Bouaoud, S.-E.; Braunstein, P.; Dusausoy, Y.; Merabet, N.; Raya, J.; Rouag, D. *J. Chem. Soc., Dalton Trans.* **1999**, 735–741.

10.1021/ic800045u CCC: $40.75
Published on Web 04/16/2008

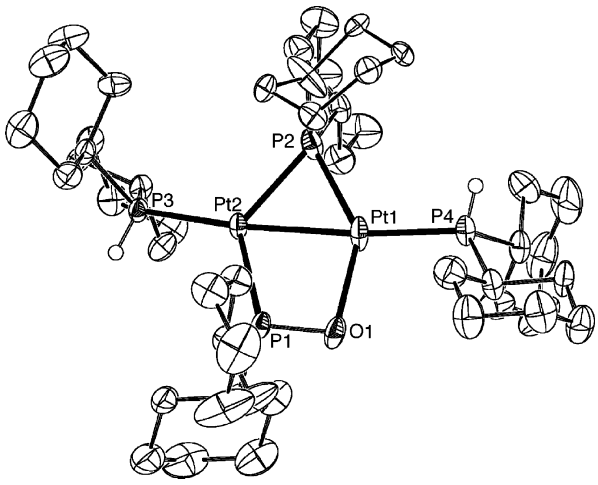

Figure 1. PLATON[5] drawing of **1**. Displacement ellipsoids are scaled to 50% probability; H atoms bonded to C and an alternative conformation in the disordered cyclohexyl ring (C19−C24) have been omitted for clarity. Interatomic distances (Å) and angles (deg): Pt(1)−O(1) 2.180(4), Pt(1)−P(2) 2.2117(19), Pt(1)−P(4) 2.2365(18), Pt(1)−Pt(2) 2.5731(16), Pt(2)−P(3) 2.2513(19), Pt(2)−P(1) 2.2860(17), Pt(2)−P(2) 2.292(2), P(1)−O(1) 1.556(4), O(1)−Pt(1)−P(2) 139.83(10), O(1)−Pt(1)−P(4) 102.47(10), P(2)−Pt(1)−P(4) 117.68(7), O(1)−Pt(1)−Pt(2) 83.26(9), P(2)−Pt(1)−Pt(2) 56.63(6), P(4)−Pt(1)−Pt(2) 174.15(4), P(3)−Pt(2)−P(1) 117.45(6), P(3)−Pt(2)−P(2) 118.73(5), P(1)−Pt(2)−P(2) 123.80(6), P(3)−Pt(2)−Pt(1) 169.59(3), Pt(1)−P(2)−Pt(2) 69.67(6).

steric requirements of the bridging phosphide force the coordination geometry of the platinum atoms to become a very distorted square planar arrangement [the angles between two adjacent atoms around the platinum centers range from 53.71(4) to 118.73(5)°]. The P−H bonds of the two $PHCy_2$ ligands are almost antiperiplanar in order to fulfill steric requirements generated by the cyclohexyl groups. The distances P(2)−Pt(1) [2.2117(19) Å] and P(2)−Pt(2) [2.292(2) Å] are different, the latter being longer as expected on the basis of the different trans influences exerted by the oxygen and phosphorus atoms. The sum of the angles at Pt indicates a perfect planarity of the Pt_2P_4O core. An analogous Pt−Pt−P−O trapezoid is found in $[(PMePh_2)Pt\{\kappa^2P,O\text{-}\mu\text{-}P(O)Ph_2\}]_2(Pt{-}Pt)$,[4] in which the two Pt atoms are bridged by two diphenylphosphinito ligands. Comparison of the two complexes shows that the bond distances of the Pt−Pt−P−O core in complex **1** are all slightly longer {for instance, the Pt−O distance is 2.180(4) Å in **1** vs 2.167(3) Å in $[(PMePh_2)Pt\{\kappa^2P,O\text{-}\mu\text{-}P(O)Ph_2\}]_2(Pt{-}Pt)$}. It is interesting to note that replacing one four-membered ring in $[(PMePh_2)Pt\{\kappa^2P,O\text{-}\mu\text{-}P(O)Ph_2\}]_2(Pt{-}Pt)$ with a three-membered ring in **1** results in a longer Pt−Pt bond {2.5731(16) Å for **1** vs 2.554(1) Å for $[(PMePh_2)Pt\{\kappa^2P,O\text{-}\mu\text{-}P(O)Ph_2\}]_2(Pt{-}Pt)$}.

Reaction with $PHCy_2$. The addition of one equivalent of $PHCy_2$ to a toluene solution of **1** caused its transformation, after 3 h at 50 °C, into the symmetric Pt^I dimer $[(PHCy_2)Pt(\mu\text{-}PCy_2)]_2(Pt{-}Pt)$ (**2**) with contemporary elimination of $P(O)HCy_2$. Complex **2** was previously obtained by us, and its spectroscopic features have been discussed elsewhere.[6] Here it is sufficient to note that substitution of the phosphinito bridge with a phosphido bridge caused the expected strong deshielding in the ^{31}P NMR signal of μ-PCy_2 (from δ 137 in **1** to δ 242 in **2**) due to the presence of two phosphides bridging two Pt atoms linked by a single bond.[7]

Monitoring the reaction mixture containing **1** and $PHCy_2$ at room temperature using $^{31}P\{^1H\}$ NMR made possible the detection in the solution of a large amount of the intermediate **3**, which started to form immediately after addition of $PHCy_2$ and progressively transformed into **2** (Scheme 1). The multinuclear NMR features of **3**[8] indicated the structure *syn*-$[(PHCy_2)_2Pt(\mu\text{-}PCy_2)Pt(PHCy_2)\{\kappa P\text{-}P(O)Cy_2\}](Pt{-}Pt)$ (**3**), the product of attack by $PHCy_2$ at Pt^1 of **1** with decoordination of the phosphinito oxygen. The fact that $PHCy_2$ attacks at Pt^1 was clearly revealed by a $^{31}P\{^1H\}$ exchange spectroscopy (EXSY) experiment performed on a C_6D_6 solution containing **1** and $PHCy_2$, which showed an exchange cross-peak between free $PHCy_2$ (δ −27.6) and P^3 of **3** (δ 38.1) (Figure S1 in the Supporting Information). The transformation of **3** into **2** can be envisaged to occur via proton transfer from P^3H to P^4O, followed by ring closure of the resulting Pt^1-PCy_2 moiety and elimination of $P(O)HCy_2$.

Reaction with $P(O)HCy_2$. When equimolar amounts of **1** and $P(O)HCy_2$ in toluene were mixed, no reaction occurred even after 10 days at 50 °C. However, using an excess of $P(O)HCy_2$ (>5 eq) caused the transformation of **1** into the hydrido-bridged complex *syn*-$[(PHCy_2)\{\kappa P\text{-}P(O)Cy_2\}Pt(\mu\text{-}PCy_2)(\mu\text{-}H)Pt(PHCy_2)\{\kappa P\text{-}P(O)Cy_2\}](Pt{-}Pt)$ (**4**) (Scheme 2). Although ^{31}P and ^1H NMR spectra of the reaction mixtures after 2 h at 50 °C showed the quantitative conversion of **1** into **4**, the purification of the product from excess $P(O)HCy_2$ required particular care. The reason for this was found in the formation of adducts of **4** with free $P(O)HCy_2$, as suggested by NMR spectroscopy. In particular, all of the signals in the $^{31}P\{^1H\}$ NMR spectrum of the mixture after reaction [which contained an excess of $P(O)HCy_2$] were very broad except for that of the bridging phosphide. The broadness of the free $P(O)HCy_2$ signal was due to an exchange process involving formation and rupture of the hydrogen bonds between free $P(O)HCy_2$ and coordinated $P(O)Cy_2$ in the adducts of **4** with free $P(O)HCy_2$; the broadness of the signals from the coordinated $P(O)Cy_2$ and $PHCy_2$ ligands had to be attributed to hindered rotation about the Pt−P bonds.[6,9] Exchange between free $P(O)HCy_2$ and coordinated $P(O)Cy_2$ could be ruled out on

(4) Alcock, N. W.; Bergamini, P.; Gomes-Carniero, T. M.; Jackson, R. D.; Nicholls, J.; Orpen, A. G.; Pringle, P. G.; Sostero, S.; Traverso, O. *J. Chem. Soc., Chem. Commun.* **1990**, 980–982.
(5) Spek, A. L. *J. Appl. Crystallogr.* **2003**, *36*, 7–13.
(6) Mastrorilli, P.; Nobile, C. F.; Fanizzi, F. P.; Latronico, M.; Hu, C.; Englert, U. *Eur. J. Inorg. Chem.* **2002**, 1210–1218.
(7) Pt^I dinuclear complexes having a planar Pt_2P_2 core are described in ref 1 and in: (a) Leoni, P.; Chiaradonna, G.; Pasquali, M.; Marchetti, F. *Inorg. Chem.* **1999**, *38*, 253–259. (b) Cristofani, S.; Leoni, P.; Pasquali, M.; Eisentraeger, F.; Albinati, A. *Organometallics* **2000**, *19*, 4589–4595.
(8) $\delta_{P(1)}$ 182.9, $\delta_{P(2)}$ 29.3, $\delta_{P(3)}$ 38.1, $\delta_{P(4)}$ 84.1, $\delta_{P(5)}$ 8.7, $^2J_{P(1),P(3)} = 228$ Hz, $^2J_{P(1),P(4)} = 255$ Hz, $^2J_{P(2),P(5)} = 210$ Hz, $^1J_{P(1),Pt(1)} = 2020$ Hz, $^1J_{P(1),Pt(2)} = 2578$ Hz, $^1J_{P(2),Pt(1)} = 2692$ Hz, $^1J_{P(3),Pt(1)} = 2990$ Hz, $^1J_{P(4),Pt(2)} = 3460$ Hz, $^1J_{P(5),Pt(2)} = 2571$ Hz; $\delta_{H-P(2)}$ 4.31, $\delta_{H-P(3)}$ 4.28, $\delta_{H-P(5)}$ 4.54, $^1J_{H,P(2)} = 318$ Hz, $^1J_{H,P(3)} = 284$ Hz, $^1J_{H,P(5)} = 313$ Hz; $\delta_{Pt(1)}$ −5030, $\delta_{Pt(2)}$ −5211.
(9) Mastrorilli, P.; Nobile, C. F.; Latronico, M.; Gallo, V.; Englert, U.; Fanizzi, F. P.; Sciacovelli, O. *Inorg. Chem.* **2005**, *44*, 9097–9104.

Scheme 1. Reaction of **1** with $PHCy_2$

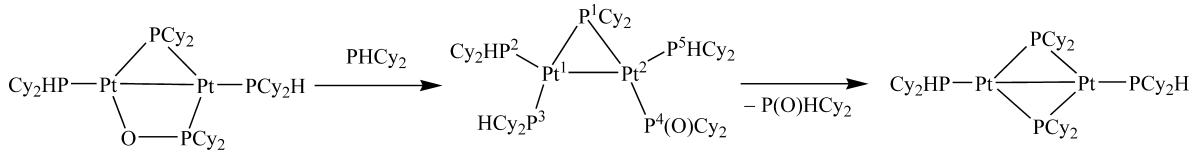

1 **3** **2**

Scheme 2. Reaction of **1** with $P(O)HCy_2$

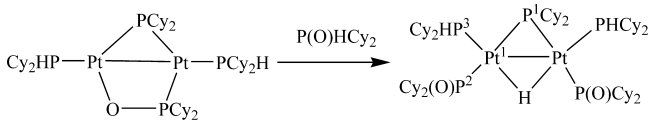

1 **4**

the basis of the relative sharpness of the phosphide signal along with the absence of cross-peaks in $^{31}P\{^1H\}$ and ^1H EXSY experiments.[10]

Addition of water to the mixture after reaction caused **4** to precipitate as a mixture of H_2O and $P(O)HCy_2$ solvates, but use of aqueous NaOH instead of pure water afforded pure **4** (as the water adduct) devoid of $P(O)HCy_2$.

The $^{31}P\{^1H\}$ spectrum (Figure 2) of **4** showed the resonance of the bridging phosphide as a triplet [with ^{195}Pt satellites; $^2J_{P(1),P(2)} = 254$ Hz, $^1J_{P(1),Pt} = 1173$ Hz] due to coupling with the phosphinito ligands in the trans positions.[11] The ^1H NMR spectrum showed only a signal attributed to the H atoms of the coordinated $PHCy_2$ ligands (δ 5.0, $^1J_{H,P} = 330$ Hz, $^2J_{H,Pt} = 60$ Hz) and a multiplet (with two sets of ^{195}Pt satellites arising from isotopomers containing one or two NMR-active Pt atoms) attributable to the bridging hydride (Figure 3a). Comparison with the $^1H\{^{31}P\}$ NMR spectrum (Figure 3b) showed that the multiplicity of the hydride signal was due only to $^1H-^{31}P$ couplings. The $^{195}Pt\{^1H\}$ NMR spectrum showed a very broad signal (δ −5467) that confirmed the presence of slowly rotating P ligands bound to Pt.

The crystal structure of **4**·$2H_2O$ is shown in Figure 4. The molecule is located on a crystallographic C_2 axis passing through the bridging phosphide and hydride ligands; it has a uniformly distributed arrangement of ten cyclohexyl groups around the Pt_2P_5 core. The dicyclohexylphosphinite ligands are oriented with both oxygens pointing out from the molecule and forming hydrogen bonds with two H_2O molecules clathrated in the crystal.[12] The Pt−Pt distance of 2.8502(6) Å is compatible with a single bond between the metal atoms (the Pt−Pt distance in platinum metal is 2.77 Å). Such a distance compares well with those found in analogous Pt dinuclear complexes having a bridging phosphide and a bridging hydride.[13]

An interesting structural feature in the solid is the formation of an extended one-dimensional chain in which complexes and water molecules interact via hydrogen bonds (Figure 5), a feature recently found in the related phosphinito platinum complexes $[Pt(L)\{(PPh_2O)_2H\}(PPh_2OH)]$ (L = C_6F_5, $C{\equiv}CBu^t$).[14] Each phosphinito oxygen atom of **4** participates in hydrogen bonds to two water molecules in general positions, thus forming an alternating sequence of one complex and two water molecules that has an overall stoichiometry of **4**·$2H_2O$.

Since dicyclohexylphosphane oxide is in tautomeric equilibrium with dicyclohexylphosphinic acid,[15] its reaction with **1** can in principle occur by attack of either the oxygen of the tetrahedral $P(O)HCy_2$ form or the phosphorus of the pyramidal $P(OH)Cy_2$ form at Pt^1. However, given that coordination to a metal stabilizes the pyramidal phosphinic acid form,[16] attack at Pt^1 by the phosphorus of the $Cy_2P(OH)$ seems more likely.

Reaction with PCy_3. The reactions of **1** with $PHCy_2$ and $P(O)HCy_2$ involve proton transfer: from $PHCy_2$ to the coordinated $P(O)Cy_2$ to release $P(O)HCy_2$ in the synthesis of **2** and from $P(O)HCy_2$ to the Pt−Pt bond to give **4**. In order to assess the reactivity of **1** with a nucleophile that does not contain an easily transferable H atom, we reacted **1** with 1 eq of PCy_3. The reaction led to nearly complete conversion of **1** into **5** (Scheme 3) after 6 h at 295 K in THF. In this case, in contrast to the reaction with $PHCy_2$, the monobridged intermediate **6**[17] shown in Scheme 3 cannot undergo proton transfer from the incoming nucleophile to the vicinal $P(O)Cy_2$. Therefore, reclosing of the phosphinito

(10) The mixing time was varied in the 10–200 ms range for both ^1H and $^{31}P\{1H\}$ EXSY experiments performed at 295 and 323 K.

(11) In these systems, the coupling constant between the phosphide and the $PHCy_2$ ligands in mutually cis positions is often negligible. See, for instance: Van Leeuwen, P. W. N. M.; Roobeek, V. F.; Frijns, J. H. G.; Orpen, A. G. *Organometallics* **1990**, *9*, 1211–1222.

(12) A dimethylphosphinito complex featuring hydrogen bonds with water molecules in the solid state has recently been reported in: Ruiz, J.; Garcia-Granda, S.; Diaz, M. R.; Quesada, R. *Dalton Trans.* **2006**, 4371–4376.

(13) (a) Jans, J.; Naegeli, R.; Venanzi, L. M.; Albinati, A. *J. Organomet. Chem.* **1983**, *247*, C37–C41. (b) Siedle, A. R.; Newmark, R. A.; Gleason, W. B. *J. Am. Chem. Soc.* **1986**, *108*, 767–773. (c) Alonso, E.; Forniés, J.; Fortuño, C.; Martin, A.; Orpen, A. G. *Organometallics* **2001**, *20*, 850–859. (d) Reference 11.

(14) Dìez, A.; Forniés, J.; Gòmez, J.; Lalinde, E.; Martìn, A.; Moreno, M. T.; Sànchez, S. *Dalton Trans.* **2007**, 3653–3660.

(15) The prototropic equilibrium of phosphane oxides has been reported to depend on the medium of the samples (see, for instance: Magiera, D.; Szmigielska, A.; Pietrusiewicz, K. M.; Duddeck, H. *Chirality* **2004**, *16*, 57–64.). We have found that in the case of dicyclohexylphosphane oxide, the phosphinic acid form is the predominant one in aromatic solvents.

(16) (a) Algarra, A. G.; Basallote, M. G.; Fernandez-Trujillo, M. J.; Hernandez-Molina, R.; Safont, V. S. *Chem. Commun.* **2007**, 3071–3073. (b) Akbayeva, D. N.; Di Vaira, M.; Costantini, S. S.; Peruzzini, M.; Stoppioni, P. *Dalton Trans.* **2006**, 389–395. (c) Nagaraja, C. M.; Nethaji, M.; Jagirdar, B. R. *Inorg. Chem.* **2005**, *44*, 4145–4147.

(17) Signals at δ 183.6 (dd, $^2J_{\mu\text{-P,PCy}_3} = 233$ Hz, $^2J_{\mu\text{-P,PO}} = 260$ Hz, μ-PCy_2), δ 85.4 [m, $^2J_{\mu\text{-P,PO}} = 260$ Hz, $P(O)Cy_2$], δ 37.5 (m, $^2J_{\mu\text{-P,PCy}_3} = 233$ Hz, PCy_3), δ 47.1 (m, $PHCy_2$), and δ 11.8 (m, $PHCy_2$) observed by monitoring the reaction solution using $^{31}P\{^1H\}$ NMR were attributed to this monobridged intermediate by comparison with the spectroscopic features of **3**.

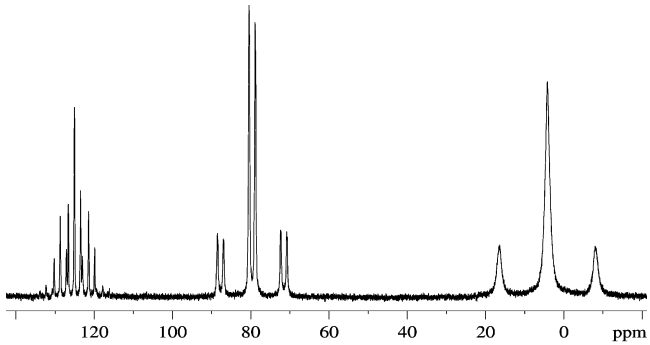

Figure 2. $^{31}P\{^{1}H\}$ NMR spectrum of **4** ($CDCl_3$, 295 K).

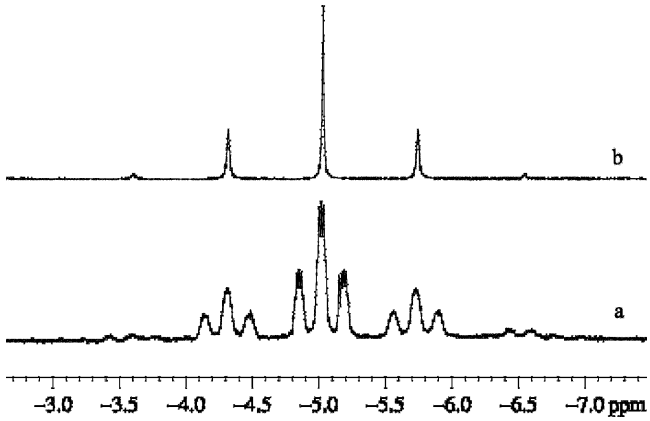

Figure 3. (a) ^{1}H and (b) $^{1}H\{^{31}P\}$ NMR spectra of **4** in the hydride region ($CDCl_3$, 295 K).

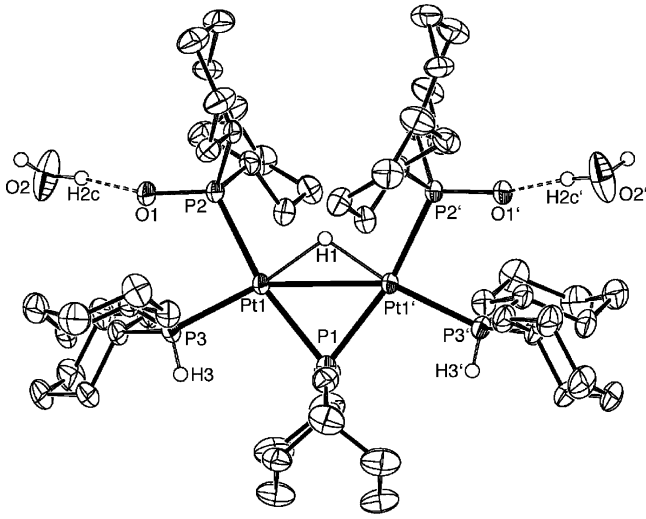

Figure 4. PLATON[5] drawing of **4**·$2H_2O$. Displacement ellipsoids are scaled to 50% probability; only the shortest hydrogen bonds have been shown. H atoms bonded to C have been omitted for clarity. Primed atoms are related to unprimed ones by the symmetry operation $1 - x, y, {}^1/_2 - z$. Interatomic distances (Å) and angles (deg): Pt(1)−P(3) 2.2428(10), Pt(1)−P(1) 2.3065(11), Pt(1)−P(2) 2.3322(11), Pt(1)−Pt(1′) 2.8502(6), P(1)−C(1) 1.850(4), P(2)−O(1) 1.526(3), Pt(1)−H(1) 1.74(4), P(3)−Pt(1)−P(1) 101.16(3), P(3)−Pt(1)−P(2) 91.46(4), P(1)−Pt(1)−P(2) 164.47(3), P(3)−Pt(1)−Pt(1′) 151.88(3), P(1)−Pt(1)−Pt(1′) 51.83(2), P(2)−Pt(1)−Pt(1′)116.52(2), P(3)−Pt(1)−H(1)168.2(12), P(1)−Pt(1)−H(1) 86.8(18), P(2)−Pt(1)−H(1) 82.2(17), Pt(1)−Pt(1′)−H(1) 35.0(18).

bridge accompanied by release of the $PHCy_2$ molecule (which is less basic than PCy_3) becomes favored.

When the reaction was carried out in toluene at 50 °C with an excess of PCy_3, formation of **5** was accompanied by an 20% yield of $[(PCy_3)Pt(\mu\text{-}PCy_2)]_2(Pt-Pt)$ (**7**), the PCy_3 analogue of **2**. The formation of **7**, which precipitates from the reaction mixture as a yellow powder, is not unexpected. In fact, the released $PHCy_2$ molecule can trigger the formation of diphosphido compounds by attacking the phosphinito-bridged species **1** and **5**, after which replacement of the residual coordinated $PHCy_2$ ligand(s) with PCy_3 occurs.

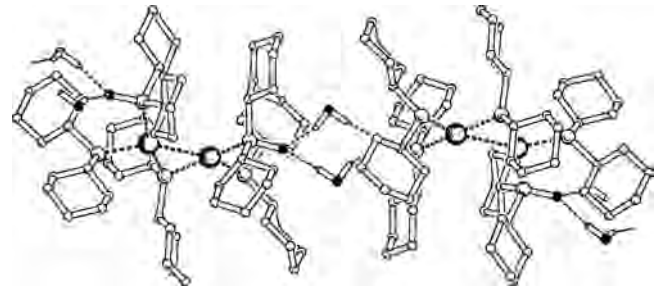

Figure 5. One-dimensional chain of complexes and water molecules in **4**·$2H_2O$. The chain extends along $[10\bar{1}]$; the view direction is [111].

Reaction with $P(S)HCy_2$. We completed this study by investigating the reactivity of **1** toward dicyclohexylphosphane sulfide, $P(S)HCy_2$, a molecule possessing two atoms (P and S) that potentially can ligate to the metal. The reaction, carried out in toluene at 50 °C, selectively gave complex **8**, in which the bridging $P(O)Cy_2$ ligand was replaced by a bridging $P(S)Cy_2$ ligand (Scheme 4).

The $^{31}P\{^{1}H\}$ NMR spectrum of **8** (Figure 6) was very similar to those of **1** and **5**, the main differences being the highfield shift of the resonance and the remarkably large value of the $^{2}J_{P,Pt}$ coupling constant of the $P(S)Cy_2$ ligand compared with those of $P(O)Cy_2$ in **1**. The sharpness of all of the $^{31}P\{^{1}H\}$ NMR signals can be taken as an indicator of the bridging coordination mode of the $P(S)Cy_2$ ligand. In fact, as in the case of **1**, the doubly bridged structure assures free rotation of the coordinated dicyclohexylphosphanes and, at the same time, a unique conformation for the $P(S)Cy_2$ ligand; both of these circumstances are compatible with sharp $^{31}P\{^{1}H\}$ NMR signals. As a result of the decreased P═S bond order, and analogous to results for other known κ^2P,S-thiophosphinito-bridged $Pt^{I}-Pt^{I}$ compounds,[18] the P═S IR stretching band of **8** (545 cm^{-1}) was red-shifted with respect to that of the free phosphane sulfide (615 cm^{-1}).

The $^{195}Pt\{^{1}H\}$ NMR spectrum of **8** (Figure 7) showed two dddd signals, one centered at δ −5218 (S-bound Pt^{1}) and the other at δ −5376 (P-bound Pt^{2}). These values compare well to those obtained for related $Pt_2\{\kappa^2P,S\text{-}\mu\text{-}P(S)R_2\}L_2$ complexes (R = Me, Ph, Cy, OEt; L = $P(OMe)_3$, $P(OPh)_3$, PPh_3, $PMePh_2$),[18c,d,19] which range from δ −5128 to −5216 and are compatible with both Pt atoms being in the +1 oxidation state.[18] In contrast to the results for **1**, each ^{195}Pt

(18) (a) Wagner, K. P.; Hess, R. W.; Treichel, P. M.; Calabrese, J. C. *Inorg. Chem.* **1975**, *14*, 1121–1127. (b) Walther, B.; Messbauer, B.; Meyer, H. *Inorg. Chim. Acta* **1979**, *37*, L525–L527. (c) Boag, N. M.; Browning, J.; Crocker, C.; Goggin, P. L.; Goodfellow, R. J.; Murray, M.; Spencer, J. L. *J. Chem. Res., Miniprint* **1978**, 2962–2983. (d) Messbauer, B.; Meyer, H.; Walther, B.; Heeg, M. J.; Rahman, A. F. M. M.; Oliver, J. P. *Inorg. Chem.* **1983**, *22*, 272–277.

(19) Zschunke, A.; Meyer, H.; Heidlas, I.; Messbauer, B.; Walther, B.; Schädler, H.-D. *Z. Anorg. Allg. Chem.* **1983**, *504*, 117–127.

Scheme 3. Reaction of **1** with PCy_3

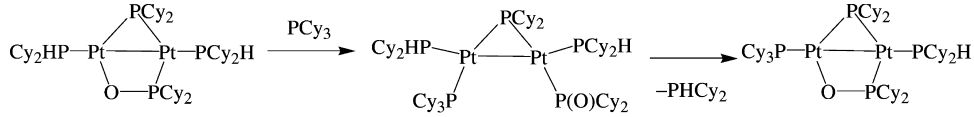

1 **6** **5**

Scheme 4. Reaction of **1** with Dicyclohexylphosphane Sulfide

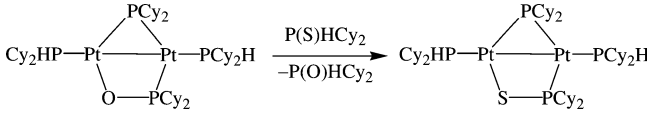

1 **8**

peak was flanked by ^{195}Pt satellites ($^1J_{Pt,Pt} = 190$ Hz, Figure 7), suggesting that replacing O with S has a pronounced effect on the types of orbitals involved in the metal−metal bond (see below).

In light of the results obtained with $PHCy_2$ and $P(O)HCy_2$, it can be presumed that $P(S)HCy_2$ attacks the Pt^1 atom, forming either intermediate **A** (S attack at Pt^1, path *a*) or intermediate **C** (P attack at Pt^1, path *b*).[20] Both intermediates could evolve into the final product **8** by hydrogen transfer to the dangling $P(O)Cy_2$ ligand (forming intermediates **B** and **D**, respectively) followed by ring closure (Scheme 5).

NMR monitoring of the reaction between **1** and $P(S)HCy_2$ did not detect any species other than reactants and **8**. Thus, we tried to distinguish between these two reaction paths by studying the reaction of **5** with $P(S)HCy_2$ (in this case, products deriving from paths *a* and *b* become distinguishable in view of the different phosphanes borne by Pt^1 and Pt^2), but the expected substitution product did not form. With the experimental data collected to this point, no definitive choice between paths *a* and *b* could be made. Thus, a DFT study aimed at elucidating the relative stabilities of the proposed intermediates was carried out.

DFT Study. Density functional theory calculations were first performed in order to study the electronic structure of complex **1** and its reactivity toward nucleophiles. Because of the large size of this complex and the computational load necessary to perform high-level calculations on several compounds, we performed preliminary calculations on three models that included increasing sizes of the substituents on the phosphane ligands. In particular, we considered ligands having (*i*) methyl, (*ii*) isopropyl, and (*iii*) the full cyclohexyl substituents on the four (two terminal and two bridging) phosphanes. Thus, geometry optimizations of the two simplified model complexes **1**-Methyl and **1**-Isopropyl and the actual complex **1** were performed. Table 1 compares the main geometrical parameters of the Pt_2P_4O core obtained from these calculations with those from the X-ray data for the actual complex.

The results showed that the geometrical parameters of the simplest model, having the small methyl substituents, were already in good agreement with the X-ray results, suggesting that inclusion of the full cyclohexyl groups on the phosphane ligands was not necessary to reproduce the electronic structure and the main geometrical features of the Pt_2P_2O core of complex **1**. Indeed, the calculated interatomic distances within the Pt_2P_4O core were only slightly (0.03–0.07 Å) larger than the X-ray values (with the greatest discrepancy, 0.07 Å, being observed only for the Pt−Pt bond), probably as a result of incomplete inclusion of the relativistic effects, which is known to lead to overestimates of metal–ligand and metal−metal bond distances. Therefore, in subsequent calculations we used only the simplified models having methyl substituents on the phosphane ligands; for the sake of simplicity, we will not distinguish between the actual cyclohexyl-substituted complexes and their methyl-substituted models in the discussion that follows.

Next we performed a Mulliken analysis of the charge distribution in complex **1** in order to align the atoms of the Pt_2P_2O core in order of increasing electron density. We found the following Mulliken gross atomic charges: $Q(Pt^1) = +0.18$, $Q(Pt^2) = -0.20$, $Q(P^1) = -0.18$, $Q(P^2) = -0.29$, and $Q(O) = -0.82$ (Figure 8). It is apparent from these values that the most electron-poor center within the Pt_2P_2O core is the O-bound Pt^1 atom while the most electron-rich center is the O atom. It is worth noting that the asymmetry of the bridging phosphinito ligand leads to an asymmetric charge distribution on the two platinum atoms, with phosphane-bound Pt^2 being significantly more electron-rich than

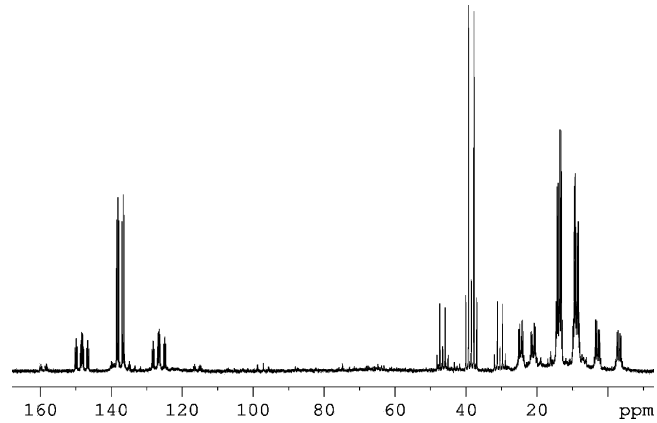

Figure 6. $^{31}P\{^1H\}$ NMR spectrum of **8** (C_6D_6, 295 K).

(20) P- or S-bound thiophosphinito complexes with several metals have been reported. Complexes with Pt: (a) Rahman, A. F. M. M.; Ceccarelli, C.; Oliver, J. P.; Messbauer, B.; Meyer, H. *Inorg. Chem.* **1985**, *24*, 2355–2359. (b) Anderson, D. M.; Ebsworth, E. A. V.; Stephenson, T. A.; Walkinshaw, M. D. *Angew. Chem., Int. Ed. Engl.* **1981**, *20*, 290–291. Complexes with W, Mo, or Cr: (c) Lindner, E.; Meier, W.-P. *J. Organomet. Chem.* **1976**, *114*, 67–87. Complexes with Mn or Re: (d) Lindner, E.; Schilling, B. *Chem. Ber.* **1977**, *110*, 3725–3732. Complexes with Mn: (e) Lindner, E.; Dreher, H. *J. Organomet. Chem.* **1976**, *104*, 331–346. (f) Lindner, E.; Dreher, H. *J. Organomet. Chem.* **1973**, *55*, 347–356. (g) Lindner, E.; Dreher, H. *Angew. Chem., Int. Ed. Engl.* **1975**, *14*, 416–417. Complexes with Cr, Mn, or Mo: (h) Lindner, E.; Meier, W.-P. *J. Organomet. Chem.* **1973**, *51*, C14–C16. Complexes with Cr or Mo: (i) Lindner, E.; Meier, W.-P. *J. Organomet. Chem.* **1974**, *67*, 277–285. Complexes with Ir: (j) Marsala, V.; Faraone, F.; Piraino, P. *J. Organomet. Chem.* **1977**, *133*, 301–305.

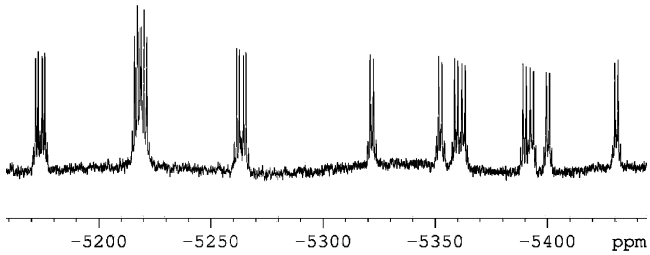

Figure 7. $^{195}Pt\{^{1}H\}$ NMR spectrum of **8** (C_6D_6, 295 K).

Scheme 5. Possible Mechanisms for Formation of **8**

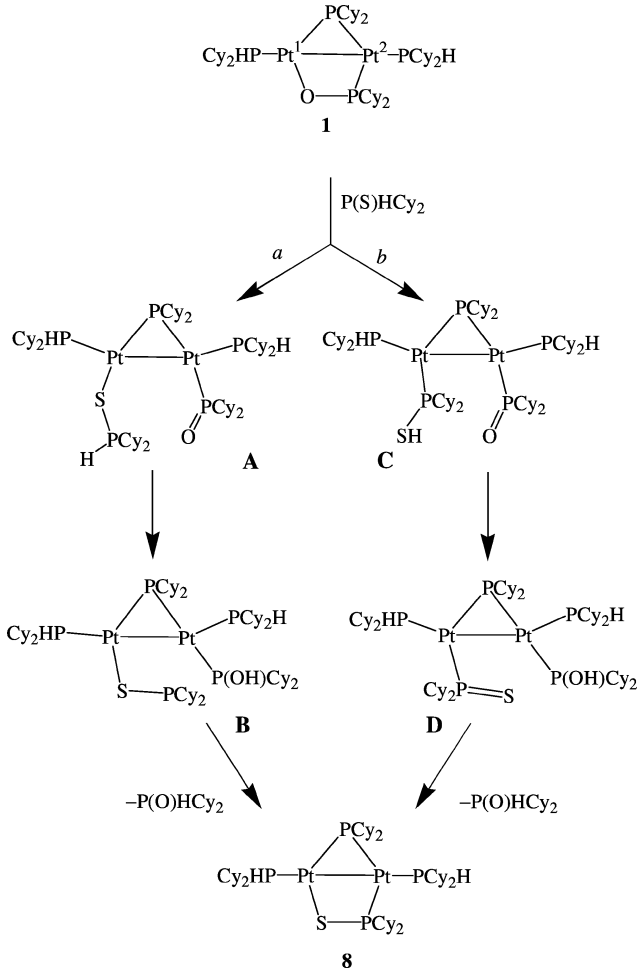

O-bound Pt^1. On the one hand, this result corroborates our starting hypothesis (based on ^{195}Pt NMR features) concerning the electrophilic character of Pt^1, while on the other hand, it predicts an amphiphilic character for **1**, suggesting that Pt^1 is the target of nucleophilic attack while O is the preferred site of electrophilic attack.[21] Indeed, the reactivity with nucleophiles discussed above (Schemes 1–4) is characterized by initial attack of the incoming nucleophile at the Pt^1 atom, leading to cleavage of the Pt^1−O bond and formation of a singly PCy_2-bridged intermediate that subsequently evolves to the thermodynamically most stable product, the nature of which depends on the nucleophile used.

DFT calculations of the structural and electronic properties of complexes **2**, **4**, and **8** (using methyl-substituted models) were also performed in order to study the effect of the different bridging ligands on the metal−metal bonding and charge distribution. The calculated values of the main interatomic distances in the Pt_2P_2S core of **8**, which are reported in Table 2, show that changing the bridging ligands does not significantly affect the metal−metal distance. In particular, the metal−metal distances slightly increased in the order **1** < **2** ≈ **8**, with all of the values being within the range of a Pt^I−Pt^I single bond. It is worth noting that the Pt−Pt bond length in **8** was only slightly (0.03 Å) longer than that in **1** in spite of the fact that the Pt−S and P−S bonds were significantly longer (by 0.2–0.5 Å) than the Pt−O and P−O bonds (see Tables 1 and 2); this indicates that a net strengthening of the Pt−Pt bond occurs upon replacement of the bridging phosphinito ligand by a thiophosphinito ligand. Moreover, the Pt−Pt bond length was slightly shorter in **1** than in **2** in spite of the presence of the longer bridging ligand κ^2P,O-μ-Cy_2PO instead of μ-PCy_2, indicating a net weakening of the Pt−Pt bond in **2**. A significantly longer Pt−Pt bond distance of 2.93 Å was calculated for **4**, in agreement with the X-ray value of 2.85 Å (in view of the expected elongation of 0.07 Å due to incomplete inclusion of relativistic effects, as also observed for **1**) and consistent with the lengthening expected upon protonation.

Table 1. Comparison of the Main Interatomic Separations (Å) Calculated for the Three Models of **1** with the Values Obtained from the X-ray Data for the Actual Complex

	Pt^1−Pt^2	Pt^1−μ-P	Pt^2−μ-P	Pt^1−O	P−O	Pt^2−P(O)
1-Methyl	2.64	2.26	2.34	2.21	1.59	2.33
1-Isopropyl	2.64	2.26	2.35	2.21	1.60	2.34
1	2.64	2.25	2.35	2.21	1.60	2.34
1 from X-ray data	2.573(2)	2.212(2)	2.292(2)	2.180(4)	1.556(4)	2.286(2)

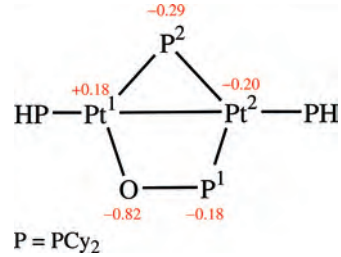

Figure 8. Mulliken gross atomic charges in the Pt_2P_2O core of complex **1**.

Energy-level diagrams for the frontier molecular orbitals (MOs) of **1**, **2**, and **8** are displayed in Figure 9. The energy-level diagram for the MOs of **2** shows the expected pattern for a dinuclear Pt^I−Pt^I complex with a metal−metal single bond.[22] Indeed, for this species, which has C_{2h} symmetry, nine of the highest-occupied MOs have predominant contributions from the metal orbitals, and each is classified according to its irreducible representation in the C_{2h} point group and the bonding character (σ, π, etc.) of the combination of metal orbitals that form it. In the coordinate system used in our calculations (see Chart 1), in which the Pt_2P_4 core lies in the *xy* plane and the two platinum atoms are located along the *y* axis, combining the two Pt $5d_{x^2-y^2}$ orbitals

(21) The reactivity of **1** toward electrophiles is currently under investigation in our laboratories.

(22) Mealli, C.; Ienco, A.; Galindo, A.; Carreño, E. P. *Inorg. Chem.* **1999**, *38*, 4620–4625.

Table 2. Interatomic Separations (Å) Obtained from DFT Calculations or X-ray Data for Complexes **2**, **4**, and **8**

	Pt−Pt	Pt−μ-P	Pt−P(H)		
2-Methyl	2.66	2.35	2.24		
	Pt^1-Pt^2	$Pt^1-\mu$-P	Pt^1-H	$Pt^1-P(H)$	$Pt^1-P(O)$
4-Methyl	2.93	2.34	1.79	2.27	2.38
4 from X-ray data	2.8502(6)	2.3065(11)		2.2428(10)	2.3322(11)
	Pt^1-Pt^2	$Pt^1-\mu$-P	$Pt^2-\mu$-P	P−S	$Pt^2-P(S)$	Pt^1-S
8-Methyl	2.67	2.27	2.33	2.10	2.33	2.42

leads to a_g and b_u MOs having σ and σ^* character, respectively. Combination of the two $5d_{yz}$ orbitals produces a_u and b_g MOs having $\pi_\perp$ and $\pi_\perp^*$ character, respectively ($\perp$ = perpendicular to the *xy* plane), while combination of the two $5d_{xy}$ orbitals yields a_g and b_u MOs having $\pi_{||}$ and $\pi_{||}^*$ character, respectively ($||$ = parallel to the *xy* plane). Combining the two $5d_{xz}$ orbitals leads to b_g and a_u MOs having δ and δ^* character, respectively, and combination of the two $5d_{z^2}$ orbitals generates set of a_g and b_u MOs having δ and δ^* character, respectively. Within the same coordinate system, the Pt−P bonds are described by orbitals having a_g and b_u symmetry that involve $5d_{xy}$, $5d_{x^2-y^2}$, 6s, and 6p metal orbitals. Among the nine occupied MOs, the four fully occupied orbitals having δ or δ^* character ($13b_g$, $14a_u$, $21a_g$, and $20b_u$) are nearly pure metal-based orbitals (>80% $5d_{xz}$ or $5d_{z^2}$) with bonding and antibonding counterparts close in energy. These four MOs are responsible for the δ-type Pt−Pt interaction; however, they are fully occupied, and there is no net δ bonding. A substantial metal contribution (70% $5d_{yz}$) is also observed for the $13a_u$ and $14b_g$ orbitals, which have $\pi_\perp$ and $\pi_\perp^*$ character, respectively, and together yield no net π bonding. The $19a_g$ and $21b_u$ MOs, which have $\pi_{||}$ and $\pi_{||}^*$ character, respectively, show a smaller $5d_{xy}$ contribution (30–60%), since they also involve platinum 6s and 6p and phosphorus 3p orbitals and describe the bonding between the Pt and bridging P atoms. They combine to give no net contribution to Pt−Pt bonding as well. The MO responsible for metal−metal bonding is $18a_g$ (not shown in Figure 9), which is located at lower energy (–7.7 eV) and has Pt−Pt σ character; the corresponding MO with σ^* character, $22b_u$, is empty. This picture shows that the Pt−Pt bond in **2** arises from the bonding σ interaction between the two $5d_{x^2-y^2}$ orbitals (with the corresponding antibonding combination σ^* being empty), which means that the bond between the two metal atoms may be qualitatively described as a single σ bond.

Similar energy-level diagrams are observed for **1** and **8** (Figure 9), even though the lower C_s symmetry of the latter compounds changes the labels of the MOs and allows a larger mixing among different d-type orbitals. The main differences are observed for MOs having σ, $\pi_{||}$, or $\pi_{||}^*$ character, which show a more extensive mixing of the $5d_{xy}$ and $5d_{x^2-y^2}$ orbitals, particularly those on Pt^1, with the 2p orbitals of oxygen or 3p orbitals of sulfur. The same is also observed for the MOs of δ^* character in which the $5d_{xz}$ orbital of Pt^1 mixes with the $2p_z$ orbital of oxygen ($3p_z$ of sulfur) to describe Pt−O (Pt−S) π bonding. These effects lead to a decrease in the Pt−Pt antibonding character of the $\pi_{||}^*$ and $\delta^*(d_{xz})$ MOs and thus suggest a slightly stronger Pt−Pt bond, in agreement with the structural evidence discussed above.

A detailed orbital analysis of the frontier orbitals of **4** has also been carried out in order to study the effect of protonation of the Pt−Pt bond on its electronic structure. The small but significant decrease of the Pt−Pt bond order upon protonation is consistent with the transformation of the two-electron, two-center (2-e, 2-c) metal−metal bond into a weaker two-electron, three-center (2-e, 3-c) bond that has been experimentally[14,16a–c] and theoretically[23] investigated. Figure 10 shows the perturbation of the frontier MOs of the symmetric $[(PHMe_2)\{P(O)Me_2\}Pt(\mu\text{-}PMe_2)Pt\{P(O)Me_2\}(PMe_2H)]^-$ fragment, **4′**, by the empty 1s orbital of the bridging proton fragment. The frontier MOs of this dinuclear fragment are similar to those of **2**, except for the C_{2v} symmetry and the smaller difference in the energies of MOs with bonding and antibonding character that results from the longer Pt−Pt bond. In a coordinate system similar to that used for **2**, having the Pt_2P_5 core in the *xy* plane and the two Pt atoms along the *y* axis, only the MOs with σ and $\pi_{||}$ character have the appropriate symmetries and sufficient overlap to interact with the empty 1s orbital of the H fragment. The in-phase combination gives rise to a 3-c Pt−H−Pt bonding orbital ($1a_1$) at low energy, while the occupied nonbonding ($2a_1$) and empty out-of-phase ($3a_1$) combinations have significantly higher energies. The resulting transfer of electron density from the metal−metal-based σ and $\pi_{||}$ orbitals to the bridging H ligand, supported by a Mulliken charge of −0.21 on the hydrogen, leads to weakening and elongation of the metal−metal bond. The slightly negative charge on the bridging hydrogen suggests behavior intermediate between those of a proton and a hydride ligand, in agreement with the relatively short Pt−Pt bond (2.850 Å), which is not completely broken as would be expected for a "true" $Pt^{II}-Pt^{II}$ dimer.

DFT calculations were eventually performed in order to elucidate the relative stabilities of the possible intermediates involved in the reaction of **1** with $P(S)HCy_2$ to give **8** (**A**−**D** in Scheme 5) and make a definitive choice between paths *a* and *b*.

Geometry optimizations of **A** and **C**, which result from the initial attack of $P(S)HCy_2$ through the S and P atoms, respectively, led to two local minima on the potential energy surface only when a conformation having the hydrogen of the $P(S)HCy_2$ ligand on Pt^1 in the anti position with respect to the oxygen atom of the $P(O)Cy_2$ ligand on Pt^2 was considered. In this case, **C** was 10.4 kcal mol^{-1} more stable in energy than **A**.

When the conformation having the hydrogen on $P(S)HCy_2$ in the syn position with respect to the oxygen atom on $P(O)Cy_2$ was considered, a barrierless proton transfer (rather than just the expected formation of a P−H···O hydrogen bond) between the two ligands occurred, and the geometry

(23) (a) Baik, M.-H.; Friesner, R. A.; Parkin, G. *Polyhedron* **2004**, *23*, 2879–2900, and references therein. (b) Bo, C.; Poblet, J.-M.; Costas, M.; Sarasa, J.-P. *J. Mol. Struct.* **1996**, *371*, 37–43. (c) Bo, C.; Costas, M.; Poblet, J. M.; Rohmer, M.-M.; Benard, M. *Inorg. Chem.* **1996**, *35*, 3298–3306.

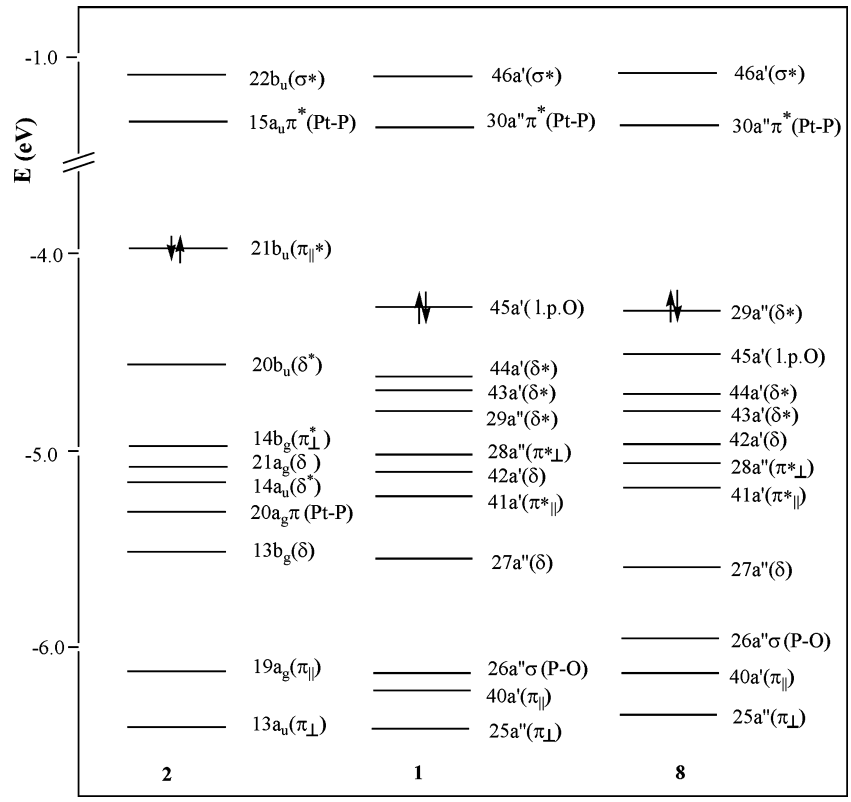

Figure 9. Energy-level diagrams for the frontier molecular orbitals of **1**, **2**, and **8**.

Chart 1. Coordinate System Used in the DFT Calculations

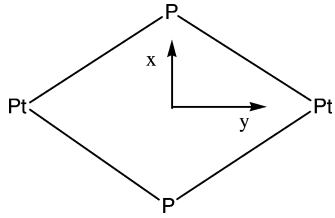

optimizations led directly to **B** and **D**. These intermediates are thus the global minima on potential energy surface for the attack of P(S)HCy$_2$ through S and P, respectively, with **D** more stable by 9.0 kcal mol^{-1}. Since **B** and **D** were 12.0 and 10.6 kcal mol^{-1} below **A** and **C**, respectively, and the only barriers for the **A** → **B** and **C** → **D** interconversions (the barriers for rotation around the Pt−P and Pt−S bonds, respectively) were negligible, **B** and **D** can be considered the only real possible intermediates (both of which rapidly evolve into **8**) in the reaction of **1** with P(S)HCy$_2$. This result indicates that attack by P(S)HCy$_2$ through the P atom is thermodynamically favored over attack through the S atom, thus suggesting that the reaction of **1** with P(S)HCy$_2$ occurs preferentially through path *b*.

Conclusions

This study revealed that the reactivity of complex **1** with molecules such as PHCy$_2$, PCy$_3$, P(O)HCy$_2$, and P(S)HCy$_2$ is governed by the electrophilicity of the O-bound Pt^1 atom, at which the incoming nucleophile attacks. In the case of PHCy$_2$ or P(S)HCy$_2$, the reaction leads to a product in which the bridging phosphinito ligand is substituted with a bridging

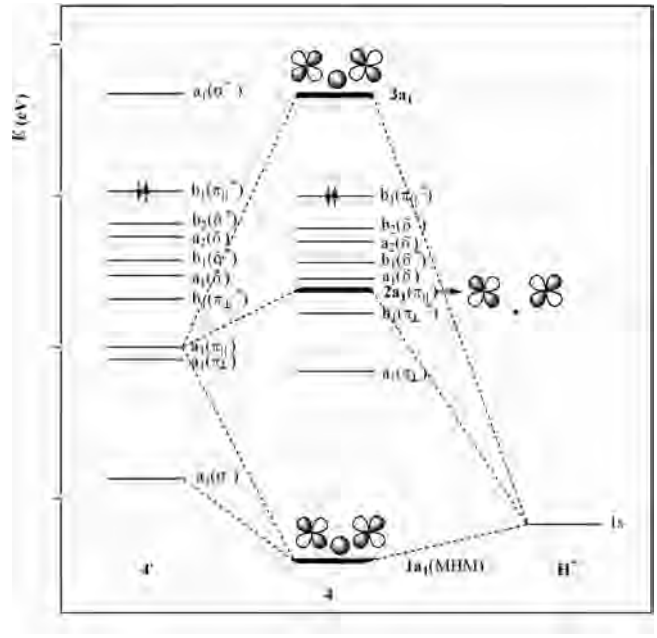

Figure 10. MO interaction diagram for **4** built from **4′** and H$^+$ fragments.

phosphido or thiophosphinito ligand, respectively. In the case of PCy$_3$, substitution of the Pt^1-bound PHCy$_2$ ligand with retention of the phosphinito bridge takes place. Finally, in the reaction with P(O)HCy$_2$, which contains an acidic proton in its P(OH)Cy$_2$ tautomeric form, formal protonation of the Pt−Pt bond occurs, yielding the hydrido-bridged dinuclear complex **4**.

In every case, the starting 30-electron structure is preserved. In particular: (*i*) the 2-e donor molecule PCy$_3$ replaces

Table 3. Crystallographic Data and Structural Refinement Details for **1** and **4**·2H_2O

	1	**4**·2H_2O
empirical formula	$C_{48}H_{90}OP_4Pt_2$	$C_{60}H_{117}O_4P_5Pt_2$
formula mass	1197.26	1447.59
temperature (K)	130(2)	110(2)
wavelength (Å)	0.71073	0.71073
crystal system	Monoclinic	Monoclinic
space group	$P2_1/c$	$C2/c$
unit cell dimensions		
a (Å)	14.548(10)	13.536(4)
b (Å)	19.811(14)	23.754(6)
c (Å)	21.225(12)	20.066(5)
β (deg)	125.31(3)	91.154(4)
V (Å^3)	4992(6)	6451(3)
Z	4	4
D_{calcd} (mg m^{-3})	1.593	1.490
absorption coeffient (mm^{-1})	5.760	4.498
θ range for data collection (deg)	2.00–29.16	1.71–27.45
total reflections	67284	41737
independent reflections	13077	7385
data/parameters	13077/541	7385/321
goodness of fit on F^2	1.027	1.052
R1[a] [$I > 2\sigma(I)$]	0.0396	0.0293
wR2[b] (all data)	0.0938	0.0781
largest diff. peak, hole (e Å^{-3})	4.936, –3.938	2.287, –0.515

[a] $R1 = \sum||F_o| - |F_c||/\sum|F_o|$. [b] $wR2 = [\sum w(F_o^2 - F_c^2)^2/\sum w(F_o^2)^2]^{1/2}$.

the 2-e donor $PHCy_2$ coordinated to the electrophilic Pt atom; (*ii*) the potentially 3-e donor molecules $PHCy_2$ and $P(S)HCy_2$ replace only one of the two 3-e donor ligands originally present in **1**, namely, $P(O)Cy_2$; (*iii*) the potentially 3-e donor $P(O)HCy_2$ fragments into two 1-e donor ligands, giving the bridging hydride addition product **4**. In this case, the κ^2P,O-μ-$P(O)Cy_2$ group is not released by the complex, but its coordination mode is changed from bidentate (a 3-e donor ligand) in **1** to monodentate (a 1-e donor ligand) in **4**.

DFT calculations confirmed the remarkable electrophilicity of Pt^1 and allowed us to clarify the nature of the metal−metal bond in several of the considered dinuclear complexes and elucidate some of their reaction pathways.

Experimental Section

Complex **1** was prepared using a slight modification of the literature procedure.[1] A solution of *cis*-[$PtCl_2(PHCy_2)_2$] (100 mg) in CH_2Cl_2 (7.0 mL) was added to a solution containing 1.0 g of NaOH, 2.0 mL of H_2O, and 7.0 mL of acetone; the resulting biphasic system was vigorously stirred at room temperature for 2 h. The yellow organic phase was separated and dried on Na_2SO_4. After filtration, the solvent was evaporated to dryness and the residue redissolved in *n*-hexane. The resulting suspension was filtered, and the filtrate was dried under vacuum, yielding 76 mg of pure **1** (85%). Dicyclohexylphosphane and tricyclohexylphosphane were purchased from Strem and used as received. Dicyclohexylphosphine oxide[24] and dicyclohexylphosphine sulfide[25] were synthesized using literature procedures. All of the manipulations were carried out under a pure dinitrogen atmosphere using freshly distilled, oxygen-free solvents. C, H, N elemental analyses were performed using a Carlo Erba EA1108 CHNS-O elemental analyzer. Infrared spectra were recorded on a Bruker Vector 22 spectrometer.

Mass spectrometry analyses were performed using a time-of-flight mass spectrometer equipped with an electrospray ion source (Bruker micrOTOF). All of analyses were carried out in positive-ion mode. The sample solutions were introduced by continuous infusion at a flow rate of 180 μL min^{-1} with the aid of a syringe pump. The instrument was operated with end-plate offset and capillary voltages set to −500 and −4500 V, respectively. The nebulizer pressure was 0.8 bar (N_2), and the drying gas (N_2) flow rate was 7.0 L min^{-1}. The capillary exit and skimmer 1 voltages were 90 and 30 V, respectively. The drying gas temperature was set at 220 °C. The software used for the simulations was Bruker Daltonics DataAnalysis (version 3.3).

NMR spectra were recorded using a BRUKER Avance DRX400 spectrometer; frequencies are referenced to Me_4Si (^1H and ^{13}C), 85% H_3PO_4 (^{31}P), and H_2PtCl_6 (^{195}Pt). Signal attributions and coupling-constant assessments were made on the basis of a multinuclear NMR analysis that included $^1H-^{31}P$ HMQC, $^1H-^{195}Pt$ HMQC, and $^{31}P\{^1H\}$ long-range COSY experiments. Coupling constants not directly extractable from the monodimensional spectra were obtained and attributed on the basis of the tilts of the multiplets due to the "passive" nuclei[26] in the aforementioned 2D spectra.

All of the calculations were performed using the Amsterdam Density Functional (ADF) package.[27–29] The inner-shell cores (1s for C and O, 1s and 2p for P, and 1s−4f for Pt) were kept frozen. Valence orbitals based on Slater-type orbitals (STOs) were expanded within a triple-ζ basis set augmented with a polarization function. The MOs for all of the main group atoms were expanded in an uncontracted triple-ζ STO basis set. For platinum orbitals, we used a double-ζ STO basis set for 5s and 5p and a triple-ζ STO basis set for 5d and 6s. As polarization functions, we used one 6p function for Pt, one 4d for P, one 3d for C, N, and O, and one 2p for H.

The local density approximation exchange correlation potential and energy were used along with the Vosko−Wilk−Nusair parametrization[30] for homogeneous electron-gas correlation, including Becke's nonlocal correction[31] to the local exchange expression and Perdew's nonlocal correction[32] to the local expression for the correlation energy. Molecular structures of all of the considered complexes were optimized at this gradient-corrected level. Since the relativistic effect is important in these Pt-containing dimers, the zero-order regular approximation (ZORA) formalism without spin–orbit coupling was included.[33,34] Previous calculations have indicated that use of gradient-corrected functionals with the ZORA approximation can reliably predict properties of metal dimers in comparison with Dirac four-component MP2 calculations.[35,36] Since the properties and reactivities of the considered complexes were investigated in the solid state or in apolar solvents, only gas-phase calculations without inclusion of any solvation effects were performed.

(24) Klaui, W.; Song, C.-E. *Inorg. Chem.* **1989**, *28*, 3845–3849.
(25) Rauhut, M. M.; Currier, H. A.; Wystrach, V. P. *J. Org. Chem.* **1961**, *26*, 5133–5135.
(26) Carlton, L. *Bruker Rep.* **2000**, *148*, 28–29.
(27) *Amsterdam Density Functional (ADF) 2004*; Scientific Computing & Modelling NV: Amsterdam, 2004; available from http://www.scm.com.
(28) Boerrigter, P. M.; te Velde, G.; Baerends, E. *Int. J. Quantum Chem.* **1988**, *33*, 87–113.
(29) te Velde, G.; Baerends, E. J. *J. Chem. Phys.* **1992**, *99*, 84–98.
(30) Vosko, S. H.; Wilk, L.; Nusair, M. *Can. J. Phys.* **1980**, *58*, 1200–1211.
(31) Becke, A. D. *Phys. Rev. A* **1988**, *38*, 3098–3100.
(32) Perdew, J. P. *Phys. Rev. B* **1986**, *33*, 8822–8824.
(33) van Lenthe, E.; Baerends, E. J.; Snijders, J. G. *J. Chem. Phys.* **1993**, *99*, 4597–4610.
(34) van Lenthe, E.; Baerends, E. J.; Snijders, J. G. *J. Chem. Phys.* **1994**, *101*, 9783–9792.
(35) Minori, A.; Sayaka, M.; Takahito, N.; Kimihiko, H. *Chem. Phys.* **2005**, *311*, 129–137.
(36) Xia, F.; Chen, J.; Cao, Z. X. *Chem. Phys. Lett.* **2006**, *418*, 386–391.

[(PHCy$_2$)Pt(μ-PCy$_2$)]$_2$(*Pt*−*Pt*) (2).[6] A solution of dicyclohexylphosphane (14.4 mg, 0.73 mmol) in toluene (2 mL) was added to a yellow-orange solution of **1** (87.0 mg, 0.073 mmol) in toluene (3 mL), and the mixture was stirred at 50 °C for 3 h. After the solution was cooled to room temperature and concentrated to 2 mL, it was stored at −18 °C for 1 month in order to precipitate the desired product as an orange solid. The solid was filtered off at −20 °C, washed with ice-cold *n*-pentane, and dried in vacuo. The yield (15 mg, 17%) is believed to be limited by isolation and not by conversion. Attempts to purify **2** by selective extraction of P(O)HCy$_2$ with methanol (other solvents, such as toluene, THF, and even alkanes, were unsuitable) were unsuccessful because addition of methanol caused the decomposition of **2**.

***syn*-[(PHCy$_2$){κ*P*-P(O)Cy$_2$}Pt(μ-PCy$_2$)(μ-H)Pt(PHCy$_2$){κ*P*-P(O)Cy$_2$}](*Pt*−*Pt*)·2H$_2$O (4·2H$_2$O).** Solid **1** (90 mg, 0.075 mmol) was added to a solution of dicyclohexylphosphane oxide (90 mg, 0.42 mmol) in toluene (0.5 mL), and the mixture was stirred at 50 °C. After 2 h of reaction, the mixture was cooled to room temperature, and aqueous NaOH (7 mg in 3 mL) was added; this sequestrated the excess P(OH)Cy$_2$, causing the precipitation of a pale-yellow solid. The product was isolated by filtration, washed with *n*-hexane, redissolved in CH_2Cl_2, and dried over Na_2SO_4. Filtration and evaporation of the solvent under high vacuum yielded 76 mg of pure **4**·2H$_2$O (70% yield) as an off-white solid. The complex is stable in air, soluble in halogenated solvents and methanol, and insoluble in toluene and *n*-hexane. Anal. Calcd for $C_{60}H_{117}O_4P_5Pt_2$ (**4**·2H$_2$O): C, 49.78; H, 8.15. Found: C, 50.11; H, 8.22.

HRMS(+) ($CHCl_3$/CH_3CN): exact mass for **4**, 1410.6724 Da; found for $[M + H]^+$, *m*/*z* 1411.6851.

IR (KBr) $\bar{\nu}$ (cm^{-1}): 2924 s, 2848 s, 2310 w (P−H), 1636 w (Pt−H−Pt), 1447 s, 1348 w, 1328 w, 1292 w, 1262 s, 1191 w, 1178 w, 1104 s, 1041 s (P═O), 917 w, 886 w, 849 m, 802 m, 733 m, 575 w, 541 m, 519 m, 462 m, 407 w, 380 w, 302 w, 254 m.

^{1}H NMR ($CDCl_3$, δ): 5.01 [m, H(3), $^1J_{H,P}$ = 330 Hz, $^2J_{H,Pt}$ = 60 Hz], −5.06 [m, H(1), $^2J_{H(1),P(3)}$ = 68 Hz, $^2J_{H(1),P(1)}$ = 14 Hz, $^2J_{H(1),P(2)}$ = 7 Hz, $^1J_{H,Pt}$ = 571 Hz].

^{31}P{^{1}H} NMR ($CDCl_3$, δ): 125.0 [t, P(1), $^1J_{P,Pt}$ = 1173 Hz, $^2J_{P(1),P(2)}$ = 254 Hz], 79.6 [d, P(2), $^1J_{P,Pt}$ = 2619 Hz, $^2J_{P(2),P(1)}$ = 254 Hz], 4.2 [br, P(3), $^1J_{P,Pt}$ = 3952 Hz].

^{195}Pt{^{1}H} NMR ($CDCl_3$, δ): −5464 (m, br).

Reaction of 1 with PCy$_3$. A solution of tricyclohexylphosphane (25 mg, 0.089 mmol) in THF (4 mL) was added to a solution of **1** (100 mg, 0.083 mmol) in THF (4 mL) at room temperature, and the mixture was stirred for 6 h. The resulting orange reaction mixture contained **5**, PHCy$_2$, and a small amount of PCy$_3$, as ascertained by multinuclear NMR spectroscopy. An HRMS(+) analysis performed on the orange solid obtained after evaporation of the solvent under vacuum showed a peak at *m*/*z* 1279.6074 that was ascribable to $[\mathbf{5} + H]^+$ (the exact mass calculated for $C_{54}H_{100}OP_4Pt_2$ is 1278.6020 Da). All attempts to separate **5** from the phosphanes were unsuccessful (Figure S5 in the Supporting Information). The following spectroscopic data were obtained for **5**:

^{1}H NMR (C_6D_6, δ): 5.64 [m, H(1), $^1J_{H,P}$ = 303 Hz, $^2J_{H,Pt}$ = 43 Hz].

^{31}P{^{1}H} NMR (C_6D_6, δ): 126.7 [ddd, P(1), $^2J_{P(1),P(2)}$ = 52 Hz, $^2J_{P(1),P(3)}$ = 225 Hz, $^2J_{P(1),P(4)}$ = 50 Hz, $^1J_{P(1),Pt(1)}$ = 4349 Hz, $^1J_{P(1),Pt(2)}$ = 2989 Hz], 97.7 [dd, P(3), $^2J_{P(3),P(1)}$ = 225 Hz, $^2J_{P(3),P(2)}$ = 27 Hz, $^1J_{P(3),Pt(2)}$ = 3013 Hz, $^2J_{P(3),Pt(1)}$ = 63 Hz], 41.9 [ddd, P(2), $^2J_{P(2),P(1)}$ = 52 Hz, $^2J_{P(2),P(3)}$ = 27 Hz, $^3J_{P(2),P(4)}$ = 111 Hz, $^1J_{P(2),Pt(1)}$ = 4243 Hz, $^2J_{P(2),Pt(2)}$ = 120 Hz], 15.4 [dd, P(4), $^2J_{P(4),P(1)}$ = 50 Hz, $^3J_{P(4),P(2)}$ = 111 Hz, $^1J_{P(4),Pt(2)}$ = 3682 Hz, $^2J_{P(4),Pt(1)}$ = 102 Hz].

^{195}Pt{^{1}H} NMR (C_6D_6, δ): −4765 [dddd, Pt(1), $^1J_{Pt(1),P(1)}$ = 4349 Hz, $^1J_{Pt(1),P(2)}$ = 4243 Hz, $^2J_{Pt(1),P(3)}$ = 63 Hz, $^2J_{Pt(1),P(4)}$ = 102 Hz, $^1J_{Pt(1),Pt(2)}$ = 72 Hz], −5246 [dddd, Pt(2), $^1J_{Pt(2),P(1)}$ = 2989 Hz, $^2J_{Pt(2),P(2)}$ = 120 Hz, $^1J_{Pt(2),P(3)}$ = 3013 Hz, $^1J_{Pt(2),P(4)}$ = 3682 Hz, $^1J_{Pt(1),Pt(2)}$ = 72 Hz].

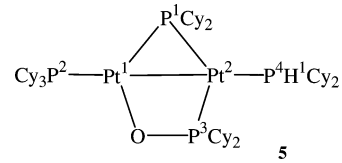

5

When the reaction was carried out in toluene at 50 °C for 2 h using a 2-fold excess of PCy$_3$, in addition to **5** the resulting mixture contained PHCy$_2$, PCy$_3$, P(O)HCy$_2$, and a significant amount (20% yield) of **7**, which was selectively precipitated upon cooling of the concentrated toluene solution at −20 °C. The following spectroscopic data were obtained for **7**:

HRMS(+) (toluene/CH_3CN): exact mass for **7**, 1344.6853 Da; found for $[M + H]^+$, *m*/*z* 1345.6889.

IR (KBr) $\bar{\nu}$ (cm^{-1}): 2924 vs, 2848 vs, 1447 vs, 1328 w, 1263 m, 1175 m, 1109 m, 1004 s, 916 w, 888 w, 849 m, 817 m, 733 m, 521 m.

^{31}P{^{1}H} NMR (C_6D_6, δ): 234.8 (t, $^1J_{P,Pt}$ = 2603 Hz, $^2J_{P,P}$ = 52 Hz, μ-PCy$_2$,), 57.8 (t, $^1J_{P,Pt}$ = 4850 Hz, $^2J_{P,P}$ = 52 Hz, $^3J_{P,P}$ = 65 Hz, PCy$_3$).

^{195}Pt{^{1}H} NMR (C_6D_6, δ): −5554 (dt, $^1J_{Pt,PCy_3}$ = 4850 Hz, $^1J_{Pt,\mu\text{-}PCy_2}$ = 2603 Hz).

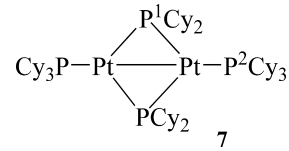

7

[(PHCy$_2$)Pt(μ-PCy$_2$){κ^2*P*,*S*-μ-P(S)Cy$_2$}Pt(PHCy$_2$)](*Pt*−*Pt*) (8). Solid **1** (72 mg, 0.060 mmol) was added to a solution of dicyclohexylphosphane sulfide (14 mg, 0.060 mmol) in toluene (2.0 mL), and the mixture was stirred at 50 °C for 3 h. After reaction, the solvent was removed under reduced pressure, and the residue was washed with methanol (3 × 1 mL) and dried under vacuum to give 64 mg of **8** (88% yield). The complex is stable in air in the solid state, very soluble in dichloromethane, toluene, and *n*-hexane, and scarcely soluble in methanol. Anal. Calcd for $C_{48}H_{90}P_4SPt_2$: C, 47.51; H, 7.48; S, 2.64. Found: C, 47.11; H, 7.59; S, 2.60.

HRMS(+) (toluene/CH_3CN): exact mass for $C_{48}H_{90}P_4SPt_2$, 1212.5009 Da; found for $[M + H]^+$, *m*/*z* 1213.4830.

IR (nujol) $\bar{\nu}$ (cm^{-1}): 2246 w (P−H), 2310 w (P−H), 545 s (P═S).

^{1}H NMR (400 MHz, C_6D_6, 295 K): δ = 5.45 [m, H(2), $^1J_{H(2),P(4)}$ = 305 Hz, $^2J_{H(2),Pt(2)}$ = 24 Hz], 4.91 [m, H(1), $^1J_{H(1),P(2)}$ = 318 Hz, $^2J_{H(1),Pt(1)}$ = 89 Hz].

^{31}P{^{1}H} NMR (161 MHz, C_6D_6, 295 K): δ = 140.8 [ddd, P(1), $^2J_{P(1),P(2)}$ = 44 Hz, $^2J_{P(1),P(3)}$ = 246 Hz, $^2J_{P(1),P(4)}$ = 50 Hz, $^1J_{P(1),Pt(1)}$ = 3794 Hz, $^1J_{P(1),Pt(2)}$ = 3234 Hz], 38.8 [d, P(3), $^2J_{P(3),P(1)}$ = 246, $^1J_{P(3),Pt(2)}$ = 2626 Hz, $^2J_{P(3),Pt(1)}$ = 255 Hz], 13.7 [dd, P(4), $^2J_{P(4),P(1)}$ = 50 Hz, $^3J_{P(4),P(2)}$ = 133 Hz, $^1J_{P(4),Pt(2)}$ = 3503 Hz, $^2J_{P(4),Pt(1)}$ = 100 Hz], 8.9 [dd, P(2), $^2J_{P(2),P(1)}$ = 44 Hz, $^3J_{P(2),P(4)}$ = 133 Hz, $^1J_{P(2),Pt(1)}$ = 3922 Hz, $^2J_{P(2),Pt(2)}$ = 124 Hz].

^{195}Pt{^{1}H} NMR (86 MHz, C_6D_6, 295 K, δ): −5218 [dddd, Pt(1), $^1J_{Pt(1),P(1)}$ = 3794 Hz, $^1J_{Pt(1),P(2)}$ = 3922 Hz, $^2J_{Pt(1),P(3)}$ = 255 Hz, $^2J_{Pt(1),P(4)}$ = 100 Hz, $^1J_{Pt(1),Pt(2)}$ = 190 Hz], −5376 [dddd, Pt(2), $^1J_{Pt(2),P(1)}$ = 3234 Hz, $^2J_{Pt(2),P(2)}$ = 124 Hz, $^1J_{Pt(2),P(3)}$ = 2626 Hz, $^1J_{Pt(2),P(4)}$ = 3503 Hz, $^1J_{Pt(1),Pt(2)}$ = 190 Hz].

X-ray Crystallography. Crystal data, parameters for intensity data collection, and convergence results for **1** and **4**·2H$_2$O are

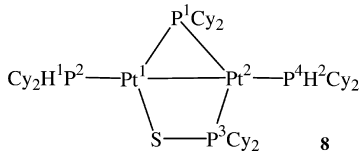

8

compiled in Table 3.[37] Diffraction-quality crystals were grown from slow evaporation of THF/*n*-hexane (**1**) and C_6D_6/*n*-hexane (**4**·$2H_2O$) mixtures. Data were collected using Mo Kα radiation (graphite monochromator, $\lambda = 0.71073$ Å) on a Bruker D8 goniometer with SMART CCD area detector on crystals having approximate dimensions of 0.27 × 0.23 × 0.17 mm (**1**) and 0.36 × 0.19 × 0.14 mm (**4**·$2H_2O$). Multiscan absorption corrections[38] (minimum and maximum transmissions, respectively, of 0.30 and 0.44 for **1** and 0.30 and 0.57 for **4**·$2H_2O$) were applied before averaging of symmetry-equivalent data ($R_{int} = 0.0596$ and 0.0493 for **1** and **4**·$2H_2O$, respectively). The structures were solved using direct methods[39] and refined using full-matrix least-squares on F^2.[40] In **1**, split positions for the atoms in the C19−C24 cyclohexyl ring were refined. In **4**·$2H_2O$, the hydride H and the hydrogen atoms associated with the water molecules were located using difference Fourier maps; the former was refined isotropically, whereas the latter were treated as riding on the water oxygens. All of the other hydrogen atoms were calculated in idealized positions and treated as riding on the closest non-hydrogen atom.

(37) Crystallographic data (excluding structure factors) for **1** and **4**·$2H_2O$ have been deposited with the Cambridge Crystallographic Data Centre as supplementary publications CCDC 657269 (**1**) and CCDC 657270 (**4**·$2H_2O$). Copies of the data can be obtained free of charge upon application to CCDC, 12 Union Road, Cambridge CB2 1EZ, U.K. [Fax: int. code +44(1223)336–033. E-mail: deposit@ccdc.cam.ac.uk.].

(38) Sheldrick, G. M. *SADABS, Program for Empirical Absorption Correction of Area Detector Data*; University of Göttingen: Göttingen, Germany, 1996.

(39) Sheldrick, G. M. *SHELXS97, Program for Crystal Structure Solution*; University of Göttingen: Göttingen, Germany, 1997.

(40) Sheldrick, G. M. *SHELXL97, Program for Crystal Structure Refinement*; University of Göttingen: Göttingen, Germany, 1997.

Acknowledgment. We thank Dr. T. Repo and Dr. M. Räisänen (University of Helsinki) for the HR ESI−MS analyses and a referee for valuable comments. The Italian MiUR is gratefully acknowledged for financial support.

Supporting Information Available: $^{31}P\{^1H\}$ EXSY spectrum of the mixture obtained after stirring of equimolar amounts of **1** and $PHCy_2$ for 1 h (Figure S1), $^{31}P\{^1H\}$ NMR spectrum of **2** (Figure S2), $^1H-^{195}Pt$ HMQC and HRMS(+) spectra of **4** (Figures S3 and S4, respectively), $^{31}P\{^1H\}$ NMR spectrum of the reaction mixture after 6 h of reaction of **1** with PCy_3 (Figure S5), $^1H-^{195}Pt$ HMQC, $^{195}Pt\{^1H\}$ NMR, and HRMS(+) spectra of **5** (Figures S6−S9, respectively), $^{31}P\{^1H\}$ NMR and HRMS(+) spectra of **7** (Figures S10 and S11, respectively), $^1H-^{195}Pt$ HMQC and HRMS(+) spectra of **8** (Figures S12 and S13, respectively), and crystallographic data in CIF format for the structural analyses of **1** and **4**·$2H_2O$. This material is available free of charge via the Internet at http://pubs.acs.org.

IC800045U